a number of latitudes in Apr. 1985. Details of the flights are contained in Table I. Figure 2 shows the derived column amounts and also amounts derived for the same days from three lines in the 1605-cm^{-1} region of NO_2 ν_3 [Fig. 1(b)], the region we previously used for the NO_2 retrievals.[8]

Good agreement is found between the amounts derived from both NO_2 bands. The error bars in Fig. 2 represent one standard deviation of the measurements in the 2915-cm^{-1} region. The variability of the 2915-cm^{-1} measurements at 70°N is substantially larger than at other latitudes for unknown reasons. The standard deviation of the 1605-cm^{-1} measurements is much smaller. There is generally overlap between the measurements in the two bands, especially when we consider that the accuracy of the line parameters is only ~10%. No systematic differences may be detected between measurements in the two bands.

Previous comparisons of stratospheric NO_2 amounts determined from simultaneous measurements (but with different instruments) in the IR ν_3 and visible regions, such as during the NASA Balloon Intercomparison Campaigns,[3] have shown significant discrepancies. However, ν_3 and visible NO_2 (nonsimultaneous) quantification from University of Denver balloon-borne measurements gave similar altitude profiles.[12] The good agreement in the present work in the retrieved amounts from the two IR bands, using the same observing instrument, supports the accuracy of the line parameters for those bands. Further intercomparison is needed to resolve differences between retrievels in the IR and visible regions.

These measurements were made with the support of the NCAR Research Aviation Facility; their assistance is acknowledged. The National Center for Atmospheric Research is sponsored by the National Science Foundation.

References

1. P. J. Crutzen, "The Influence of Nitrogen Oxides on the Atmospheric Ozone Content," Q. J. R. Meteorol. Soc. **96**, 320 (1970).
2. "Atmospheric Ozone 1985, WMO *Global Ozone Research and Monitoring Report, No. 16*, (Geneva, World Meteorological Organization), see especially Appendix B: Spectroscopic Database, Infrared to Microwave."
3. H. K. Roscoe *et al.*, "Intercomparison of Remote Measurements of Stratospheric NO and NO_2," in preparation, (1986).
4. L. S. Rothman *et al.*, "AFGL Trace Gas Compilation: 1982 Version," Appl. Opt. **22**, 1616 (1983).
5. C. Camy-Peyret, J.-M. Flaud, A. Perrin, and K. Narahari Rao, "Improved Line Parameters for the ν_3 and $\nu_2 + \nu_3 - \nu_2$ Bands of $^{14}N^{16}O_2$," J. Mol. Spectrosc. **95**, 72 (1982).
6. C. Camy-Peyret, J.-M. Flaud, J. Laurent, and G. M. Stokes, "First Infrared Measurements of Atmospheric NO_2 from the Ground," Geophys. Res. Lett. **10**, 35 (1983).
7. W. G. Mankin, "Airborne Fourier Transform Spectroscopy of the Upper Atmosphere," Opt. Eng. **17**, 39 (1978).
8. M. T. Coffey, W. G. Mankin, and A. Goldman, "Simultaneous Spectroscopic Determination of the Latitudinal, Seasonal and Diurnal Variability of Stratospheric N_2O, NO, NO_2, and HNO_3," J. Geophys. Res. **86**, 7331 (1981).
9. A. Perrin, J.-M. Flaud, C. Camy-Peyret, "Calculated Line Positions and Intensities for the $\nu_1 + \nu_3$ and $\nu_1 + \nu_2 + \nu_3 - \nu_2$ Bands of $^{14}N^{16}O_2$," Infrared Phys. **22**, 343, (1982).
10. V. Malathy Devi *et al.*, "Tunable Diode Laser Spectroscopy of NO_2 at 6.2 μm," J. Mol. Spectrosc. **93**, 179 (1982).
11. V. Malathy Devi, B. Fridovich, G. D. Jones, D. G. S. Snyder, and A. Neuendorffer, "Temperatures Dependence of the Widths of N_2-Broadened Lines of the ν_3 Band of $^{14}N^{16}O_2$," Appl. Opt. **21**, 1537 (1982).
12. A. Goldman, F. G. Fernald, W. J. Williams, and D. G. Murcray, "Vertical Distribution of NO_2 in the Stratosphere as Determined from Balloon Measurements of Solar Spectra in the 4500 Å Region," Geophys. Res. Lett. **5**, 257 (1978).

Extinction boundary value algorithms for lidar inversion

James D. Klett

PAR Associates, 1741 Pomona Drive, Las Cruces, New Mexico 88001.
Received 2 January 1985.
0003-6935/86/152462-03$02.00/0.

The familiar solution to the single-scattering lidar equation predicts extinction as a function of range in terms of (1) the relative signal strength and (2) a reference or boundary value of extinction that is present as an independent constant of integration. For cases of low visibility the solution is only weakly dependent on this latter parameter, but it can become of critical importance for some circumstances of moderate to high visibility.

Algorithms to estimate the extinction boundary value by making use of knowledge of the absolute power level of the return signal are available in the literature.[1-3] This Letter presents an alternative set which has been selected on the grounds of simplicity and performance in numerical experiments. The result is a combination of three models, one valid for cases of low optical depth, another suitable for most cases of moderate to large optical depth, and a third provided largely as a default procedure for somewhat anomalous situations that cannot be handled by either of the two principal algorithms.

On making the usual assumption that the atmospheric backscatter and extinction coefficients, β and σ, are related according to a power law of the form

$$\beta = B\sigma^k, \tag{1}$$

where B depends on wavelength and various properties of the obscuring aerosol and $k \approx 1$, the single-scattering lidar equation may be expressed in the form

$$S(r) \equiv \ln[r^2P(r)] = C + k \ln\sigma - 2\int_0^r \sigma dr'. \tag{2}$$

In this equation $P(r)$ is the instantaneous power received from range r, and the system constant C is given by

$$C = \ln(0.5P_0Bc\tau A), \tag{3}$$

where P_0 is the transmitted power, c is the velocity of light, τ is the pulse duration, and A is the effective system receiver area.

For constant k the stable solution to Eq. (2) is

$$\sigma(r) = \frac{\exp[(S - S_m)/k]}{\left\{\sigma_m^{-1} + \frac{2}{k}\int_r^{r_m} \exp[(S - S_m)/k]dr'\right\}}, \tag{4}$$

where $S_m = S(r_m)$, $\sigma_m = \sigma(r_m)$, and $r \le r_m$.[4] Note that the solution depends on both the relative signal, $S - S_m$, and the extinction boundary value σ_m; the latter makes its appearance as an independent constant of integration, as described above.

From Eq. (2) one can attempt to relate σ_m to the signal strength returned from the maximum useful range r_m:

$$S_m = C + k \ln\sigma_m - 2\int_0^{r_m} dr'. \quad (5)$$

However, the contribution of the integral attenuation term over the interval $(0,r_0)$, where r_0 is the point of transmitter and receiver beam overlap, is unfortunately unknown. Two previously made assumptions about this unknown attenuation term are that (1) the extinction is constant over the interval $(0,r_0)$[2] and (2) the average extinction over $(0,r_m)$ is the same as that over (r_0,r_m)[1].

On the other hand, the contribution to the attenuation term over the interval (r_0,r_m) is easily expressed as a function of σ_m by integration of Eq. (4):

$$\int_{r_0}^{r_m} \sigma dr' = \frac{k}{2} \ln\left\{1 + \frac{2\sigma_m}{k}\int_{r_0}^{r_m} \exp[(S - S_m)/k]dr'\right\},$$

$$= \frac{k}{2}\ln(1 + I\Omega_m). \quad (7)$$

In this last expression the extinction boundary value and the signal integral have been expressed in dimensionless form:

$$I \equiv (r_m - r_0)^{-1}\int_{r_0}^{r_m} \exp[(S - S_m)/k]dr', \quad (8)$$

$$\Omega_m \equiv 2\sigma_m(r_m - r_0)/k. \quad (9)$$

Note that Eq. (9) provides a measure of optical depth over the interval (r_0,r_m).

If we now impose the second of the assumptions described above concerning the attenuation to the crossover point, namely, that

$$\int_0^{r_m} \sigma dr' = [r_m/(r_m - r_0)]\int_{r_0}^{r_m} \sigma dr', \quad (10)$$

one arrives at the following equation for Ω_m[1]:

$$G_m = \ln\Omega_m - \frac{r_m}{(r_m - r_0)}\ln(1 + I\Omega_m), \quad (11)$$

where the constant G_m is given by

$$G_m \equiv (S_m - C)/k + \ln[2(r_m - r_0)/k]. \quad (12)$$

Thus the desired Ω_m is located at the intersections of the curve $y_1 = G_m$ with the curve (see Fig. 1)

$$y_2 = \ln\Omega - \frac{r_m}{(r_m - r_0)}\ln(1 + I\Omega).$$

However, it can be seen from the figure that there are no roots if G_m is greater than the maximum of Eq. (11) occurring at

$$\Omega_c = (r_m - r_0)/r_0 I. \quad (13)$$

Computational experience with the algorithm also shows it to be unreliable for some cases of low visibility. This might be expected from Fig. 1, since the intersection of the two curves for large Ω_m occurs where they are nearly parallel; hence a small error in the estimated value of the system constant, for example, might produce a very large error in the root.

Because of these difficulties (the possibility of there being no solution if the computed value of G_m is sufficiently in error and the possible error amplification in cases of large optical depth), it has been found useful to employ instead three separate estimation procedures, with each taylored for a range of parameters or set of conditions. For low visibilities, we note from Eq. (7) that the average value of extinction depends primarily on the relatively large magnitude of the signal integral I, so that an additional constraint is needed to select a unique boundary value of extinction. This suggests the simple approach of determining the boundary value in such cases by setting it equal to the average extinction. Then directly from Eq. (7) one obtains Ω_m as the solution to

$$\Omega_m = \ln(1 + I\Omega_m). \quad (14)$$

It is easy to show that this equation always has a solution for $I > 1$ and that it may be obtained in a few iterations starting with an initial small value for Ω_m. Any error in the estimate supplied by Eq. (14) will make little difference in the calculated visibility for the circumstances for which this particular algorithm is intended.

For high visibilities the choice of σ_m influences $\sigma(r)$ more strongly, there being insufficient optical depth for the well-known self-convergence property of Eq. (4) to play a significant role. Also, as can be seen from the large intersection angle of the curves in Fig. 1 for the case of the small root, errors in G_m will not be reflected as greatly amplified errors in the root. Hence an alternative to Eq. (14) is appropriate for high visibilities. Although Eq. (11) is suitable for this purpose, a slightly simpler algorithm may be obtained from Eq. (5) by using the previously mentioned alternative assumption of constant extinction from the lidar to the crossover point. Then Eq. (5) may be expressed in the form

$$G_m' = G_m + 2r_0\sigma_0/k = \ln\Omega_m - \ln(1 + I\Omega_m). \quad (15)$$

This equation may now be solved for the desired extinction boundary value (in dimensionless form):

$$\Omega_m = [\exp(-G_m') - I]^{-1}. \quad (16)$$

This algorithm is very similar to Mulders's[3] modification of the formulation of Ferguson and Stephens.[2]

In general σ_0 is not known unless σ_m is, but in practice this minor difficulty can be overcome through simple iteration of Eq. (16). For example, one may initially set $\sigma_0 = 0$ and solve for σ_m; then from Eq. (4) evaluated at r_0 a new value of σ_0 is obtained, which may be substituted back into Eq. (16) and so forth. This procedure is successful in the presence of errors because of the stability of Eq. (4).

As an example of a case not solvable by either the high or low visibility algorithms, consider an extinction distribution for which $I < 1$. Ordinarily, this would be interpreted as a typical low optical depth or high visibility situation, and so Eq. (16) would be applied. But if the system constant C is significantly in error, a realistic possibility, it may happen that $\exp(-G_m') < I$, so that Eq. (16) fails completely. One would, therefore, consider turning to Eq. (14), but this option also would fail since for $I < 1$, Eq. (14) has no solution except $\Omega_m = 0$. The failure of Eq. (16) to provide a solution corresponds graphically to having the line $y_1 = \Omega_m$ situated higher

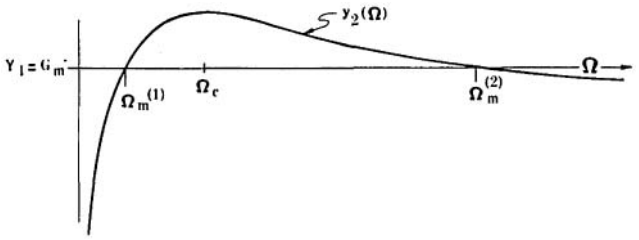

Fig. 1. Plot of $y_1 = G_m$ and y_2, given by the right-hand side of Eq. (11), showing the location of the boundary values at the intersections of the curves.

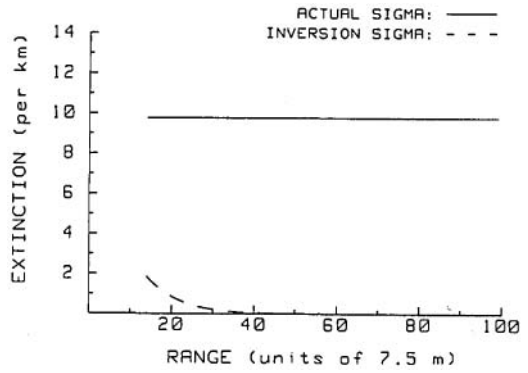

Fig. 2. Constant input distribution and the inversion solution having an unrealistic drop-off with range. Both profiles can be used to generate the same calibrated signal.

than the maximum in the curve y_2. This suggests a simple default strategy to resolve the impasse: make the estimate

$$\Omega_m = \Omega_c \tag{17}$$

in case the high and low visibility algorithms have no solutions.

The ability of the above algorithms to estimate extinction boundary values from input calibrated signals has been tested numerically using several extinction distributions and assumed errors in the system constant C. From these simulations, selection rules for the various algorithms have been obtained. They may be summarized as follows: The inversion of a lidar signal begins by trying the high-visibility algorithm first. It is considered successful if $\exp(-G_{m'}) > I + 0.01$ [see Eq. (16)] and if the resulting $\sigma_m > 0.01$ and $\sigma_0/\sigma_m < 50$. Otherwise, a switch to the low-visibility algorithm [Eq. (14)] is made, unless $I < 1$, in which case the default algorithm [Eq. (17)] is used.

From the discussion so far the above selection rules should seem reasonable, except perhaps for the criterion that Eq. (16) is to be rejected if $\sigma_m < 0.01$ or $\sigma_0/\sigma_m > 50$. These slightly arbitrary conditions have come about somewhat paradoxically from trying to apply Eq. (16) to cases of high extinction and are a consequence of the fact that in such cases there are two possible roots to Eq. (16), one very small and easily computed, and the other large and computationally unreliable due to instabilities of the kind already discussed.

Probably the easiest way to appreciate the problem of double-valuedness is to consider the lidar signal at the crossover point r_0. At that location and if the assumption of constant extinction on the interval $(0,r_0)$ is assumed, the signal S can be seen from Eq. (2) to have the following form:

$$S_0 = C + k \ln\sigma_0 - 2\sigma_0 r_0. \tag{18}$$

Therefore, σ_0 is given by the intersection of the curve $f1 = (S_0 - C)/k$ = constant with the curve $f2(x) = \ln x - x/x_c$, where $x_c = k/2r_0$ is the location of the maximum of $f2$. The situation is entirely analogous to that illustrated in Fig. 1; and, in particular, there are two roots for σ_0. Consequently, Eq. (16) may converge to a σ_m corresponding to the physically unreasonable very small root to Eq. (18). This in fact will happen for large optical depths, because the high-visibility algorithm is iterated starting with $\sigma_0 = 0$, as described earlier. The outcome can then be used as an indicator that the high-visibility algorithm is inappropriate for the particular signal being analyzed and should be rejected in favor of the low-visibility algorithm.

As a simple example of this behavior, consider the case of a cosntant extinction distribution of magnitude 9.78/km. For $k = C = 1$ and with $r_0 = 15$ range point units, the signal value computed from Eq. (18) for this distribution is $S_0 = 1.227$, so that $f2(x) = \ln x - x/4.76 = 0.227$. This equation has the two roots $\sigma_{01} = 1.85$ and $\sigma_{02} = 9.78$. The high-visibility algorithm converges to a boundary value corresponding to the smaller root. The boundary value obtained in this fashion is extremely small: $\sigma_m = 8.8 \times 10^{-6}$/km. The resulting inversion extinction profile assuming no errors in k or C is shown in Fig. 2. It should perhaps be emphasized that this profile reproduces the input signal just as well as the desired alternative constant distribution $\sigma = 9.78$/km, and so can only be rejected on the basis that it is physically implausible.

Numerical experiments with a wide range of extinction distributions, and including errors in the calibration information, show that the overall extinction boundary value algorithm obtained through use of the selection rules is capable of providing better results than previously reported individual estimation schemes.

Part of this research was performed under contract to the U.S. Army Atmospheric Science Laboratory, White Sands Missile Range, NM 88002.

References

1. J. D. Klett, "Lidar Calibration and Extinction Coefficients," Appl. Opt. **22**, 514 (1983).
2. J. A. Ferguson and D. H. Stephens, "Algorithm for Inverting Lidar Returns," Appl. Opt. **22**, 3673 (1983).
3. J. A. Mulders, "Algorithm for Inverting Lidar Returns: Comment," Appl. Opt. **23**, 2855 (1984).
4. J. D. Klett, "Stable Analytical Inversion Solution for Processing Lidar Returns," Appl. Opt. **20**, 211 (1981).
5. J. D. Klett, "Estimation of Extinction Boundary Values for Lidar Inversion," ERADCOM Report ASL-CR-85-0093-1, U.S. Army Atmospheric Sciences Laboratory, White Sands Missile Range, White Sands, NM 88002 (1985), 45 pp.

Internal and near-surface scattered field of a spherical particle at resonant conditions: comments

Ramesh Bhandari

New Mexico State University, Physics Department, Applied Lasers/Optics Group, Las Cruces, New Mexico 88003.

Received 7 April 1986.
0003-6935/86/152464-03$02.00/0.

The paper[1] by Chylek *et al.* appeared recently in *Applied Optics*. The internal electric field of a dielectric sphere is a popular topic which has received a lot of attention in the recent past.[2,3] The purpose of this Letter is to comment on certain features of internal electric field intensity reported in Ref. 1.

We first note that in Ref. 1 light incident on a dielectric sphere is assumed to be unpolarized. If the direction of incident beam is taken to be the z axis, the unpolarized light can be considered to be an incoherent equal mixture of light polarized in the x and y directions. Since the x and y directions for the polarization of incident light yield similar results in the determination of electric field intensity $|\mathbf{E}|^2$, we shall for the purpose of discussion assume that the incident